

Non-LTE Abundances and Consequences for the Evolution of the α -elements in the Galaxy

T. Idiart, F. Thévenin

Universidade de São Paulo, IAG, Depto. de Astronomia

Av. Miguel Stefano 4200, São Paulo 01065-970, Brazil

Observatoire de la Côte d'Azur

B.P. 4229, 06304 Nice Cedex 4, France

Received _____; accepted _____

ABSTRACT

Abundances of α -elements such as Ca and Mg in disk and halo stars are usually derived from equivalent widths lines measured on high resolution spectra, and assuming Local Thermodynamic Equilibrium (LTE) . In this paper, we present non-LTE differential abundances derived by computing the statistical equilibrium of CaI and MgI atoms, using high resolution equivalent widths available in the literature for 252 dwarf to subgiant stars. These non-LTE abundances combined with recent determination of non-LTE abundances of iron, seem to remove the dispersion of the [Ca/Fe] and [Mg/Fe] ratios in the galactic halo and disk phases, revealing new and surprising structures. These results have important consequences for chemical evolution models of the Galaxy. In addition, non-LTE abundance ratios for stars belonging to the M92 cluster apparently have the same behavior. More high resolution observations, mainly of globular clusters, are urgently needed to confirm our results.

Subject headings: stars: non-LTE abundances – chemical evolution – Galaxy – globular clusters

1. Introduction

The determination of abundances of nuclear species at distinct locations in the Galaxy (e.g. halo, disk and bulge) comes mainly from the spectra of late-type star atmospheres. Measured abundances in cool stars at different stages of evolution give not only the understanding of stellar nucleosynthesis, but also provide valuable information about the process of chemical enrichment of the Galaxy.

The archaeological tracers of the chemical evolution of a star system are the elements produced by explosive nucleosynthesis in type II (SNII) and type Ia (SNIa) supernovae events. The interest using such elements as tracers rests on the fact that SNII and SNIa progenitors have different lifetimes; SNII is the final evolution of massive stars and SNIa is a possible final result of evolution of a close binary system of intermediate mass stars. SNII contribute to the enrichment of the interstellar medium (ISM) mainly with elements produced by the capture of α particles (α elements) and from the r-process, and SNIa produce elements belonging to the Fe peak. Consequently, the basic tools to constraint the evolution of ISM in the Galaxy are usually the analysis of relations between ratios of heavy elements [element/Fe] and Fe abundance [Fe/H].¹

A first glance at the temporal behavior of α elements shows that the ratio [α /Fe] is approximately constant for halo metal-poor stars ([Fe/H] \leq -1.5) and decreases for metal-rich stars ([Fe/H]>-1.5) belonging to the disk. This is reasonably explained by the chemical evolutionary models that assume progressive enrichment of ISM by supernovae: first generation of stars have in their atmospheres the signature of SNII events only (called halo-phase of the Galaxy) and the subsequent generations have a signature of both SNII and SNIa events (disk-phase).

¹[Fe/H] = $\log(N_{\text{Fe}}/N_{\text{H}}) - \log(N_{\text{Fe}}/N_{\text{H}})_{\odot}$.

However, a more precise analysis of $[\alpha/\text{Fe}]$ vs. $[\text{Fe}/\text{H}]$ shows a pronounced scatter, mainly in the region of metal-poor stars. This scatter has been interpreted mostly as a consequence of the inhomogeneity of the matter having made stars rather than resulting of poor observational data (Audouze and Silk 1996).

The derivation of abundances based on the analysis of high resolution stellar spectra is usually made under the assumption of Local Thermodynamical Equilibrium (LTE). In the last 15 years, many efforts to estimate errors on abundance determinations caused by LTE assumption have been done. Recently results for Ba II (Gigas 1986, 1988, Mashonkina & Bikmaev 1996), Sr II (Belyakova & Mashonkina 1997), Na I (Mashonkina et al. 1993), Mg I (Gigas 1986, Mashonkina et al. 1996), Ca I (Drake 1991), B I (Kiselman & Carlsson 1996), Al I (Baumuller & Gehren 1997) and Fe I and Fe II (Thévenin & Idiart 1999, TI99), O I (Mishenina et al. 1999) and Mg I (Zhao, Butler & Gehren 1998) demonstrate that most lines can formed far from LTE conditions. So, some important questions arise: what is the influence of non-LTE abundance calculations on the chemical evolution diagrams of the Galaxy? Do these computations add another different constraints to the chemical history of enrichment of the matter in the Galaxy?

In this work, we present non-LTE abundances derived from computation of statistical equilibrium of Ca and Mg atoms, using published equivalent widths (Sect. 3). The atomic data and stellar atmospheric models used are presented in Sect. 2. α elements like Mg and Ca have well-known enhanced abundances in atmospheres of F-G metal-poor dwarf stars as a result of cumulative stellar generations. Recently, Nissen & Schuster(1997) and Jehin et al. (1999) proposed the existence of two sequences of stars having two different $[\alpha/\text{Fe}]$ ratios for intermediate stars ($[\text{Fe}/\text{H}] \approx -1$). Their works are based on highly accurate observations of stars having approximately same temperatures and surface gravities. Based on our non-LTE computations, we found different branches or sub-populations of stars

not only for intermediate metallicities; consequences for chemical evolution models of the Galaxy are presented in Sect. 4. We drawn our conclusions in Sect. 5.

2. Atomic data and stellar atmospheric models

The code we used to solve the equations of statistical equilibrium and radiative transfer is the 2.2 version (1995) of MULTI (Carlsson 1986). This code allows us to obtain theoretical spectra of Mg I and Ca I for given stellar atmospheric models and atomic data.

The atomic models used are shown by Grotrian diagrams presented in Figs. 1 and 2, for Mg I and Ca I respectively. We included all the fine structure levels of Mg I below 6eV: 103 levels + continuum and 980 radiative transitions. For calcium, the model has 83 levels + continuum and 483 radiative transitions. We used the atomic energy level tables given by Hirata & Horagushi (1995) (HH95) and Martin et al. (1985). Oscillator strengths are from HH95, Kurucz (1993) and Thévenin (1989, 1990). We followed the procedure described in TI99 for the remaining atomic data: radiative and collisional damping coefficients, excitation and ionization collisional cross-sections. Photoionization cross-sections are from TopBase. The van der Waals damping for all Mg lines was calculated using the approximation given by Unsöld (1955) and multiplied by a factor 1.3 as in TI99. For Ca we followed Cayrel et al. (1996). Note that the factor 1.3 is only important for strong saturated lines. As will be seen in sect. 3, we always tried to use lines lying on the linear part of the curve of growth, where this factor does not play an important role.

Stellar atmospheric models are generated using the Gustafsson et al. (1975) and Bell et al.'s grids (1976), in order to be consistent with TI99, using T_{eff} from Thévenin (1998) and $\log g$ and $[\text{Fe}/\text{H}]$ corrected for non-LTE effects from TI99. We also estimated non-LTE $\log g$ and $[\text{Fe}/\text{H}]$ values for an additional sample of stars not analyzed in TI99 (see Table 1).

Some objects, to which more accurate equivalent widths were recently available, non-LTE surface gravities and [Fe/H] were re-estimated (see Table 1). We emphasize that we do not intend to obtain absolute abundance values (see sect. 3), thus in a first approximation we can use LTE atmospheric models and perform our analysis just estimating non-LTE effects in statistical equilibrium.

3. Non-LTE calculation and results

To estimate Ca and Mg non-LTE abundances we used published equivalent widths (EW) for 252 stars, including dwarfs, subdwarfs and some subgiants. Sources of EW data are listed in Table 2 with the respective wavelengths of lines used in our analysis. Since we chose to work with one or two lines at maximum, we selected unsaturated and not very weak lines in order to have a more precise abundance determination.

To obtain non-LTE abundances we iterate MULTI with different abundance values until we reproduce the measured EW. This kind of procedure has two basic problems: 1) Our atomic model is not perfect, since, for example we do not take into account all the levels and line transitions of all spectroscopic terms and certainly there are uncertainties in oscillator strengths and in collisional processes with neutral H and He (see TI99, for a discussion). 2) Observational errors in EW measurements and inhomogeneity of EW from different sources (e.g observations with different instruments and different placement of the continua).

In order to avoid systematic effects between EW existing in the literature we renormalized our resulting abundances using common stars (comparison objects) present in the data set of different authors. Of course, a standard procedure of renormalization requires a choice of comparison objects according to each spectral type of the analyzed

stars. In our case this step was not necessary, since our selected stars have roughly the same surface gravities (dwarfs and subgiants) and a narrow range of not very cool effective temperatures ($5300 < T_{\text{eff}} < 6300$).

All the stars were renormalized to a given reference system, referred here as Ed93 system (which is based on abundances derived from published EW set of Edvardsson et al. 1993). First, we recalculate solar Ca, Mg and Fe abundances using MULTI and EW taken from Ed93. These values are our solar references. Then we estimate the relative abundances [Ca/H] and [Mg/H] for Ed93 stars. In principle, this differential procedure also allows us to minimize the imperfections of the atomic models used here. To renormalize the data from other sources we used observed common stars, as mentioned in the preceding paragraph. For example, for Mg abundance and mean metallicity $<[Fe/H]> \approx -1$ to include the data of Jehin et al. (J99) into the Ed93 system, nine common stars between these two data sets were taken, and the average of the differences between estimated abundances was calculated. This averaging procedure was used to transform J99 data to the Ed93 system. The same procedure was performed on data given by Nissen & Schuster (NS97). For metal-poor stars more steps were performed. For the Zhao & Magain (ZM90) data, for example, we renormalized ZM90 into J99 (1 common star), and ZM90 into NS97 (2 common stars), then, as J99 and NS97 have common stars with the Ed93 system, these 2 sequences gave us a renormalization ZM90-Ed93.

The main goal of this procedure is to have a homogeneous table of derived non-LTE abundances. Results are presented in Table 3 for Ca and Mg. Fig. 3 shows the abundance ratios [Ca/Fe] and [Mg/Fe] for halo and disk phases, presenting parallel structures in both evolutive diagrams.

Errors are hard to estimate because they involve many factors as described previously. We estimated the uncertainties in our abundance determinations caused by the scatter

on derived abundances when varying different parameters: stellar (T_{eff} , $\log g$ and $[\text{Fe}/\text{H}]$) and observational (EW). Fig. 4 shows the percentage errors on $\log(N_{\text{Ca}})$ and $\log(N_{\text{Mg}})$ abundances, corresponding to an incertitude in a given atmospheric parameter. These error estimates are made for a star of $\theta_{\text{eff}}=0.85$, $\log g=4.2$ and $[\text{Fe}/\text{H}]=-2.0$, for different abundance ratios $[\text{Ca}/\text{Fe}]$ and $[\text{Mg}/\text{Fe}]$, for CaI and MgI lines of table 2. We see that abundance variations are, on the average, more sensitive to uncertainties in T_{eff} , reaching a maximum of 2.2% for some CaI lines. We note that in the case of $\log g$ and $[\text{Fe}/\text{H}]$, the scatters adopted are the classical LTE errors, so the abundance errors can be overestimated.

A similar analysis is made for EW uncertainties using the same Ca I and Mg I lines. Fig. 5 shows the percentage errors in EW if we have errors in abundance ratios of the order of the structure separations ($\approx 0.15, 0.2$ dex in halo phase) displayed in Fig. 3. For example, the EW of CaI $\lambda\lambda 4578.56$ and MgI $\lambda\lambda 4571.1$ lines from Zhao & Magain 1990 have respectively EW errors of 40% and 75% when $[\text{Ca}/\text{Fe}]$ and $[\text{Mg}/\text{Fe}]$ have variations between 0.15 and 0.2 dex. The magnitude of these uncertainties are much greater than the observational errors estimated by EW sources, demonstrating that these structures can be real.

Fig. 3 confirms that effects of data renormalization as sources of these structures can be discarded, since the data of distinct sources are distributed in different parallel structures. As mentioned above, scattering in abundances is sensitive to temperature variations, however this effect seems to be not strong enough to form these structures, as can be seen in Fig. 6 that shows no correlation between abundance ratios and temperatures.

One should have also to keep in mind that such uncertainties in T_{eff} or $\log g$ result in variations on iron abundances of the same magnitude and sign as for Ca and Mg abundances, which minimize uncertainties in the abundance ratios. Thus, one can say that the ratios $[\text{Ca}/\text{Fe}]$ and $[\text{Mg}/\text{Fe}]$ are less sensitive to these uncertainties on the stellar

fundamental parameters.

4. Discussion

The two non-LTE chemical diagrams in Fig. 3 show up that the chemical enrichment of the matter in the Galaxy may be not so simple as adopted today. On [Ca/Fe] diagram, parallel structures appear: a) halo phase shows three well defined structures separated by ≈ 0.15 dex and some Ca very deficient stars. b) in the disk phase ($-0.7 < [\text{Fe}/\text{H}] < 0.4$) one can distinguish at least 4 structures. This behavior is also present in the intermediate phase of the Galaxy ($-1.2 < [\text{Fe}/\text{H}] < -0.7$), but only on 3 incurved structures.

The [Mg/Fe] diagram shows the same structures but with a greater scatter. This scatter can be due essentially for two reasons. The first one, because measured EW for magnesium lines are more imprecise (there are fewer clean weak lines in observed spectra) than for calcium lines and the second, because there are some differences between the mechanisms of Mg and Ca yields production by SNI I of distinct progenitor masses. Fig. 7 shows a pronounced scatter in [Mg/H] and [Ca/H] relation in the halo phase.

Clearly, the structures pointed out by Nissen & Schuster (1997) and Jehin et al.(1999) are present in our Calcium and Magnesium diagrams, and now extend to the disk and the halo phases of the Galaxy. Flat structures of $[\alpha/\text{H}]$ ratios vs $[\text{Fe}/\text{H}]$ are consistent with the idea that both elements come from massive supernovae. The question is: how field star formation can produce these structures if, at first, halo stars were formed independently in all the protogalaxy phase?

The existence of such structures and dichotomy exist also in Globular Clusters, as it has been demonstrated since more than 15 years. Calcium branch dichotomy in ω Cen revealed possible self-enrichment due to SN II, postulating two epochs of star formation

separated by a hiatus time. Detailed discussion of Norris, Freeman, & Mighell (1996) rejects with convincing arguments a merger origin of the dichotomy of [Ca/H] abundances in globular clusters. Another intriguing coincidence is the bimodality of C and N abundances on the main sequence of 47 Tuc (Cannon et al. 1998). As suggested by the authors, an hybrid accretion-enrichment model could help to understand how globular clusters form and the role played by stellar winds and those of SN II. Recently Boesgaard et al. (1998) have observed six turn-off stars in M92, an old very metal-poor cluster. Keeping in mind that the quality of the spectra is low, giving large uncertainties to possible derived chemical abundances from them, we derived non-LTE abundances for iron, calcium and magnesium. As an exercise, we plotted the Ca and Mg ratios for these six stars on our diagram and discovered after renormalisation that they lie exactly at the same place as halo stars. To conclude that this is more than a coincidence is premature but raises an interesting possibility: a common origin of field and globular cluster stars. If such observations could be repeated in other globular clusters for main sequence stars with better signal-to-noise ratios, then they would probably help greatly in the understanding of the formation of the Galaxy. Possible consequences could also be derived concerning the first stars in the protogalaxy as discussed by Cayrel (1986).

Another possible scenario of the formation of the Galaxy that can produce these structures in the halo phase is an incomplete mixing of SNII yields, as suggested by Karlsson & Gustafsson (1999). In an even more recent paper, Argast et al. (1999) have explored this scenario in more detail. Surprisingly, the model proposed by Argast et al. produces structures in the [Ca/Fe] and [Mg/Fe] diagrams ($[Fe/H] < -1.5$) similar to ours, as shown in Fig. 3. Their theoretical [Mg/Fe] diagram also shows greater scatter than the [Ca/Fe] diagram, suggesting that the origin of this difference is mainly the yield production mechanism (see Argast et al. 1999 for more details), as mentioned in the second paragraph of this section.

For the disk phase, observed structures have a smaller separation, and are more evident in the [Ca/Fe] diagram than in the [Mg/Fe] diagram. One interesting question is: how can chemical evolution models reproduce this result for disk metal rich stars? Is it that the mixing time scale of enriched gas was larger than the formation time of each generation of stars in the disk, as supposed for the halo phase? Observations of open cluster stars could verify if they have similar behavior of globular cluster stars.

5. Conclusions

We report here non-LTE differential abundances for 252 subdwarf to subgiant stars using published high resolution equivalent widths. [Ca/Fe] and [Mg/Fe] diagrams show remarkable structures, both in the halo and disk phases of the Galaxy, which are not related with observational or atmospheric parameter uncertainties. These results lead us to a possible evolutive galactic scenario of non-homogeneity or incomplete mixing of synthesized SNII yields (Karlsson & Gustafsson, 1999, Argast et al. 1999). A surprising result is the behavior of M92 stars, mainly in the Ca diagram, suggesting a common origin for field and cluster stars. Spectroscopic high resolution with good S/N of stars in clusters are needed to confirm or not the sketch of a new chemical evolution model presented in this work. New non-LTE analysis for other α -elements is also necessary to verify if this structural behavior applies to all α -capture SNII products.

We thank the referee for many fruitful comments and suggestions and for drawing our attention to the paper by Argast et al. T.I. acknowledges the Brazilian agency FAPESP for the grant 97/13083-7 at IAG. This work has been performed using the computing facilities provided by the program Simulations Interactives et Visualisation en Astronomie et Mécanique (SIVAM) at the computer center of the Observatoire de la Côte d’Azur.

REFERENCES

- Argast, D., Samland, M., Gerhard,O.E., Thielemann,E.-K., astro-ph/9911178
- Audouze, J., Silk, J., 1995, ApJ, 451, L49
- Baumuller, D., Gehren, T., 1997, A&A, 325, 1088
- Bell, R.A., Eriksson, K., Gustafsson, B., Nordlund, A., 1976, A&AS, 23,37
- Belyakova, E.V., Manshonkina, L.I., 1997, Astron. Rep. 41, 530
- Boesgaard, A.M., Deliyannis, C.P., Stephens, A., King, J.R., 1998, ApJ, 493, 206
- Cannon, R. D.,Croke, B.F.W., Bell, R.A., Hesser, J.E., Stathakis, R.A., 1998, MNRAS, 298, 601
- Cayrel, R., 1986, A&A, 168, 81
- Cayrel, R., Faurobert-Scholl, M., Feautrier, N., Spielfiedel, A., Thévenin, F., 1996, A&A, 312, 549
- Carlsson, M., 1986, Uppsala Astronom. Obs.Rep.33
- Carney, B.W., Wright, J.S., Sneden, C., Laird, J.B., Aguilar, L.A., Latham, D.W., 1997, AJ, 114, 363
- Drake, J.J., 1991, MNRAS, 251, 369
- Edvardsson, B., Andersen, J., Gustafsson, B., Lambert, D., Nissen, P., Tomkin, J., 1993, A&A, 102, 603
- Gigas, D, 1986, A&A, 165, 170
- Gigas, D, 1988, A&A, 193, 264
- Gustafsson, B., Bell, R. A., Eriksson, K., Nordlund, A., 1975, A&A, 42, 407
- Hirata, R., Horaguchi, T., 1995, Catalogue of Atomic Spect. Lines, VI/69

- Jehin, E., Magain, P., Neuforge, C., Noels, A., Parmentier, G., Thoul, A.A., 1999, A&A, 341, 241
- Karlsson, T., Gustafsson, B., 1999, to appear in Colloquim n=35 Liège: The galactic halo: from globular clusters to field stars
- Kiselman, D., Carlsson, M., 1996, A&A, 311, 680
- Kurucz, R., 1993, CD-Rom 13 (Cambridge: Smithsonian Astrophys. Obs.)
- Mashonkina, L.I., Bikmaev, I.F., 1996, Astron. Rep., 40, 94
- Mashonkina, L.I., Sakhibullin, N.A., Shimanskii, V.V., 1993, Astron. Rep. 37, 192
- Mashonkina, L.I., Shimanskaya, N.N., Sakhibullin, N.A., 1996, Astron. Rep. 40, 187
- Martin, W.C., Kaufman, V., Zalubas, R., Musgrove, A., Sugar, J., Corliss, C., 1985, J. Phys. Chem. Ref. Data, 10, 195
- Mishenina, T.V., Korotin, S.A., Klochkova, V.G., Panchuk, V.E., 1999, A&A, submitted
- Nissen, P., Schuster, W.J., 1997, A&A, 326, 751
- Norris, J.E., Freeman, K.C., Mighell, K.J., 1996, ApJ, 462, 241
- North, P., Berthet, S., Lanz, T., 1994, A&AS, 103, 321
- Perrin, M.N., 1986, A&A, 159, 239
- Peterson, R., 1976, ApJ, 206, 800
- Peterson, R., 1978, ApJ, 222, 181
- Peterson, R., Carney, B., 1979, ApJ, 231, 762
- Ryan, S.G., Norris, J.E., Bessell, M.S., 1991, AJ, 102, 303
- Thévenin, F., 1989, A&AS, 77, 137
- Thévenin, F., 1990, A&AS, 82, 179

Thévenin, F., 1998, Bull. du CDS n=49, Catalogue III/193

Thévenin, F., Idiart, T., 1999, ApJ, 521, 753

Tomkin, J., Lambert, D., Balachandran, S., 1985, ApJ, 290, 289

Unsöld, A., 1955, Physik der sternatmospheren (Berlin: Springer)

Zhao, G., Butler, K., Gehren, T., 1998, A&A, 333, 219

Zhao, G., Magain, P., 1990, A&AS, 86, 85

Fig. 1.— Level and Grotrian diagrams of Ca I atom.

Fig. 2.— Level and Grotrian diagrams of Mg I atom.

Fig. 3.— Chemical evolution diagrams for non-LTE CaI and MgI abundances estimated in this work and non-LTE [Fe/H] by TI99. Distinct symbols refer to EW sources indicated by the legend above. North94, Per86 and Tom95 are represented with the same symbols (hollow circles)

Fig. 4.— Percentage errors ϵ on CaI and MgI logarithmic abundances in function of atmospheric parameters variation, for different lines of a star with $\theta_{\text{eff}}=0.85$, $\log g=4.2$ and $[\text{Fe}/\text{H}]=-2.0$. These lines were used for abundance estimates of metal-poor stars (see table 2). The variation of atmospheric parameters T_{eff} , $\log g$ and $[\text{Fe}/\text{H}]$ adopted here are the classical LTE errors, and are on each corresponding diagram. Circles, up and down triangles represent respectively $[\text{Ca}/\text{Fe}] = +0.1, +0.25, +0.45$ and $[\text{Mg}/\text{Fe}] = +0.6, +0.16, -0.17$.

Fig. 5.— Percentage errors in EW in function of variations of 0.15-0.2 dex in the abundance ratios $[\text{Ca}/\text{Fe}] = +0.25$ and $[\text{Mg}/\text{Fe}] = +0.225$, for same lines in Fig. 4.

Fig. 6.— Chemical abundance ratios in function of effective temperature ($\theta_{\text{eff}} = 5040/T_{\text{eff}}$). Different symbols follow the same legend of Fig. 3.

Fig. 7.— Relation between Mg and Ca abundances. Different symbols follow the same legend of Fig. 3.

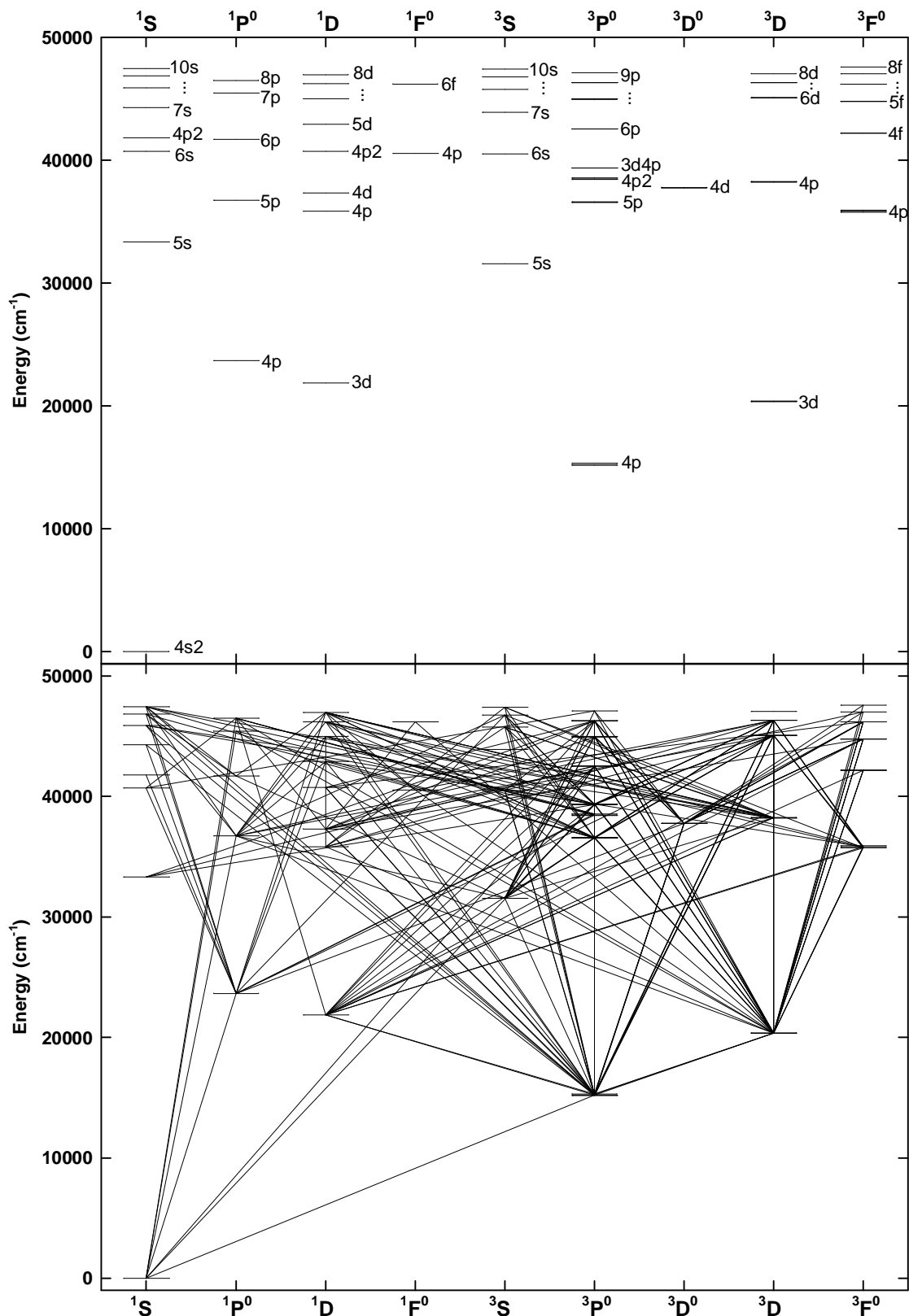


FIGURE 1

TABLE 1

ADDITIONAL AND RE-ESTIMATED ATMOSPHERIC PARAMETERS (COMPLEMENT OF TABLE 1 OF TI99)

Star	θ_{eff}	$\log g_{\text{NLTE}}$	[Fe/H] _{NLTE}
HD 3158	0.790	4.20	0.08
HD 3268	0.820	4.10	-0.13
HD 3567	0.827	4.20	-1.05
HD 4307	0.890	3.90	-0.17
HD 5015	0.810	4.10	0.10
HD 6582	0.950	4.67	-0.56
HD 6920	0.870	3.90	-0.05
HD 7476	0.770	4.15	-0.09
HD 7570	0.830	4.30	0.18
HD 9562	0.870	3.80	0.20
HD 9826	0.830	4.00	0.08
HD 10307	0.850	4.40	0.08
HD 12042	0.810	4.20	-0.22
HD 14214	0.830	4.10	0.15
HD 15335	0.860	4.20	-0.08
HD 15798	0.780	3.95	-0.10
HD 16673	0.800	4.40	0.10
HD 17288	0.882	4.32	-0.75
HD 17820	0.868	4.21	-0.54
HD 19994	0.830	4.10	0.18
HD 20807	0.840	4.50	-0.05
HD 22001	0.740	4.10	-0.01
HD 22484	0.840	4.20	0.00
HD 22879	0.861	4.35	-0.67
HD 23754	0.750	4.10	0.16
HD 24339	0.854	4.31	-0.48
HD 25621	0.800	4.00	0.16
HD 25704	0.856	4.35	-0.68
HD 26491	0.880	4.20	-0.08
HD 29645	0.840	4.10	0.16
HD 30562	0.860	4.00	0.22
HD 30743	0.780	4.20	-0.21
HD 33256	0.780	4.00	-0.14
HD 33608	0.760	4.10	0.37
HD 34411	0.860	4.10	0.09
HD 35296	0.790	4.30	0.10
HD 38393	0.790	4.30	0.00
HD 41330	0.850	4.10	-0.07
HD 43042	0.770	4.30	0.12
HD 43318	0.790	4.10	-0.03
HD 45701	0.870	4.20	0.20
HD 49933	0.760	4.20	-0.27
HD 50223	0.760	4.10	-0.04
HD 55575	0.850	4.00	-0.21
HD 59984	0.860	4.02	-0.62
HD 60532	0.820	3.92	-0.07
HD 61902	0.832	4.11	-0.59
HD 63077	0.880	4.33	-0.66

TABLE 1—*Continued*

Star	θ_{eff}	$\log g_{\text{NLTE}}$	[Fe/H] _{NLTE}
HD 63598	0.872	4.15	-0.73
HD 67228	0.870	4.20	0.14
HD 68456	0.770	4.10	-0.15
HD 70110	0.850	4.40	0.12
HD 76151	0.880	4.50	0.10
HD 78747	0.888	4.02	-0.61
HD 76932	0.860	3.75	-0.73
HD 79028	0.860	4.20	0.00
HD 79601	0.882	4.01	-0.53
HD 83220	0.777	4.20	-0.40
HD 86728	0.880	4.00	0.20
HD 87141	0.790	4.20	0.15
HD 88737	0.820	4.10	0.26
HD 88986	0.870	4.00	0.04
HD 89125	0.820	4.30	-0.24
HD 89744	0.800	4.10	0.28
HD 91752	0.780	3.90	-0.13
HD 91889	0.820	4.20	-0.11
HD 95128	0.860	4.30	0.04
HD 95241	0.860	4.10	-0.16
HD 97320	0.840	4.32	-1.02
HD 98991	0.760	4.00	0.00
HD 99747	0.760	4.00	-0.36
HD 102574	0.830	4.00	0.22
HD 102634	0.790	4.20	0.30
HD 102870	0.830	4.20	0.22
HD 103723	0.836	4.28	-0.61
HD 105004	0.864	4.28	-0.64
HD 106038	0.834	4.37	-1.07
HD 106516	0.804	4.37	-0.52
HD 107213	0.790	4.10	0.36
HD 108309	0.870	4.20	0.15
HD 108954	0.830	4.40	0.00
HD 109358	0.850	4.40	-0.05
HD 111971	0.857	4.21	-0.58
HD 112164	0.850	4.00	0.32
HD 113083a	0.859	4.42	-0.78
HD 113083b	0.874	4.42	-0.76
HD 113679	0.881	4.16	-0.45
HD 114642	0.790	3.90	-0.05
HD 114710	0.840	4.40	0.15
HD 115383	0.840	4.10	0.12
HD 115617	0.900	4.50	0.02
HD 120559	0.934	4.37	-0.78
HD 121004	0.886	4.41	-0.57
HD 121370	0.830	3.80	0.35
HD 124570	0.810	4.20	0.17
HD 124850	0.810	4.20	-0.05

TABLE 1—*Continued*

Star	θ_{eff}	loggnLTE	[Fe/H]NLTE
HD 125184	0.910	3.90	0.23
HD 126681	0.900	4.37	-0.96
HD 126793	0.871	4.10	-0.63
HD 127334	0.900	4.00	0.16
HD 128167	0.750	4.40	-0.29
HD 128620	0.880	4.20	0.20
HD 131117	0.840	4.10	0.22
HD 136064	0.820	4.10	0.10
HD 136351	0.790	4.00	0.10
HD 137052	0.790	4.00	-0.05
HD 141004	0.850	4.00	-0.01
HD 142860	0.800	4.00	-0.06
HD 143761	0.780	4.40	-0.12
HD 144585	0.860	4.00	0.29
HD 151769	0.780	3.80	0.15
HD 152924	0.822	4.05	-0.57
HD 153597	0.800	4.40	-0.04
HD 156098	0.780	3.90	0.19
HD 159332	0.800	3.90	-0.06
HD 160032	0.760	4.10	-0.16
HD 163989	0.820	3.90	-0.05
HD 165908	0.840	4.35	-0.40
HD 168151	0.770	4.15	-0.19
HD 169830	0.790	4.20	0.20
HD 173667	0.800	4.20	-0.06
HD 175317	0.760	3.20	0.25
HD 177565	0.900	4.20	0.07
HD 181096	0.800	4.20	-0.13
HD 187013	0.810	4.00	-0.06
HD 187691	0.820	4.40	0.18
HD 189558	0.895	4.11	-0.94
HD 193901	0.883	4.69	-0.90
HD 194598	0.851	4.50	-0.96
HD 196378	0.830	4.20	-0.30
HD 196892	0.850	4.28	-0.85
HD 199289	0.867	4.40	-0.89
HD 199623	0.800	4.20	-0.21
HD 200790	0.820	4.10	0.03
HD 203608	0.824	4.51	-0.52
HD 210855	0.810	3.90	0.18
HD 213657	0.830	3.94	-1.75
HD 215257	0.873	4.01	-0.67
HD 216385	0.820	4.10	-0.18
HD 217014	0.870	4.20	0.16
HD 218470	0.770	4.20	-0.04
HD 241253	0.854	4.45	-0.87
BD+20 3603	0.840	4.30	-2.04
BD+80 245	0.933	3.70	-1.78

TABLE 1—*Continued*

Star	θ_{eff}	$\log g_{\text{NLTE}}$	[Fe/H] _{NLTE}
BD-21 3420	0.848	4.31	-0.88
CD-33 3337	0.850	4.02	-1.16
CD-45 3283	0.890	4.58	-0.72
CD-47 1087	0.879	4.33	-0.64
CD-57 1633	0.850	4.30	-0.73
CD-61 0282	0.853	4.45	-0.97
G005-040	0.859	4.22	-0.68
G046-031	0.837	4.43	-0.61
G088-040	0.845	4.18	-0.64
G90-3	0.876	4.28	-1.95
G102-020	0.935	4.50	-0.93
G125-64	0.892	5.45	-2.16
G190-15	1.008	5.20	-2.65
G182-31	0.840	4.38	-2.18
W 7547	0.804	3.99	-0.30
M92-18	0.845	4.33	-2.45
M92-21	0.848	4.29	-2.38
M92-34	0.864	4.18	-2.43
M92-46	0.846	4.23	-2.41
M92-60	0.831	4.33	-2.40
M92-350	0.851	4.28	-2.38

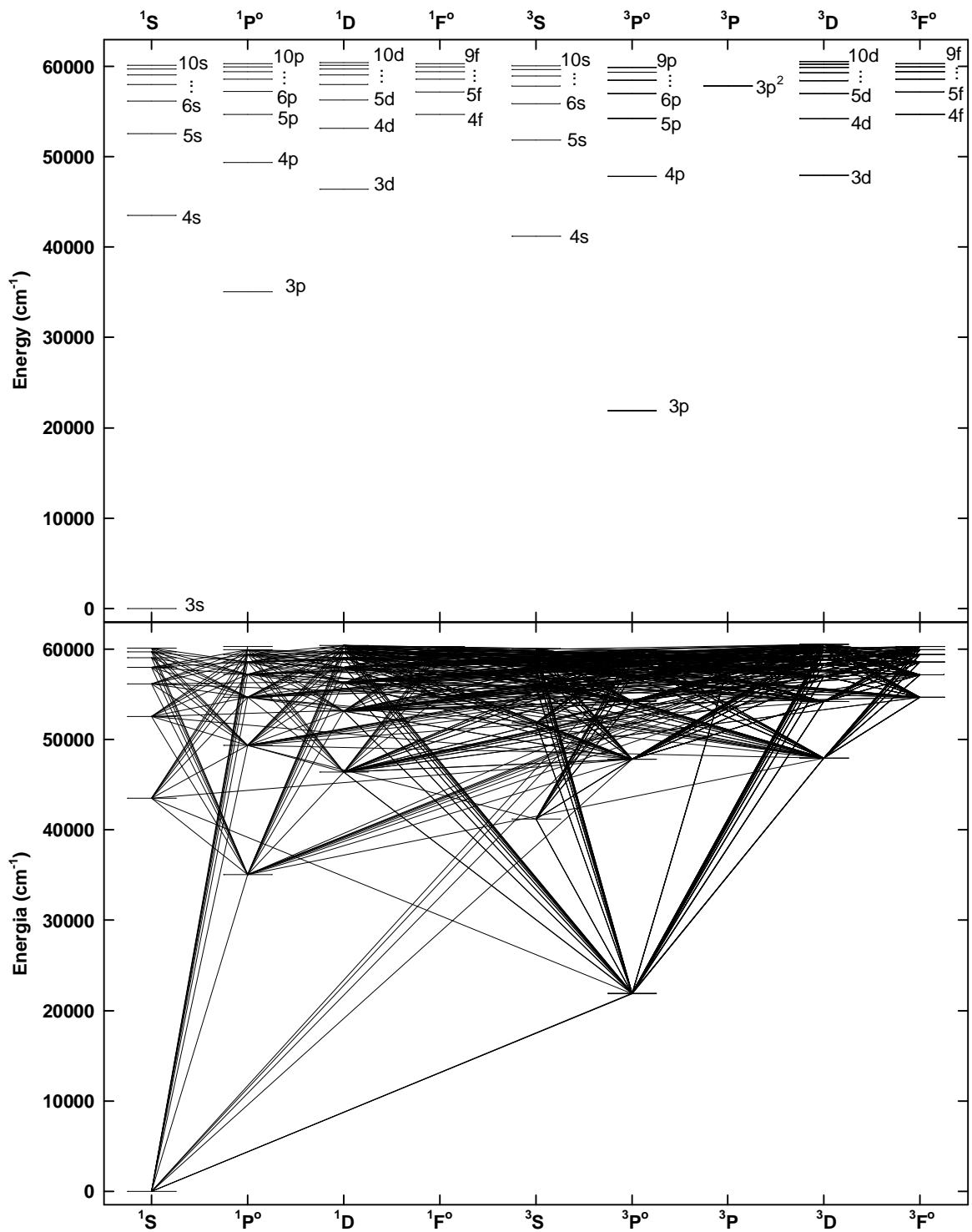


FIGURE 2

TABLE 2
SOURCES OF OBSERVED EW OF SELECTED LINES

EW references	Ca I lines (Å)	Mg I lines (Å)
Edvardsson et al. 1993 (Ed93)	6166.44	8717.82
Nissen & Schuster 1997 (NS97)	6166.44	5711.1
Jehin et al. 1999 (J99)	4578.56	4571.10
Zhao & Magain 1990 (ZM90)	4578.56	4571.1
Ryan et al. 1991 (R91)	4283.01,4302.52 4318.65,4454.78	4167.27
Carney et al. 1997 (C97)	6102.70	5528.42
Boesgaard et al. 1998 (B98)	6161.30	4702.99
Peterson 1976,1978,1979 (Pet76,Pet78,Pet79)	4425.44,4435.68	4571.10
Tomkin et al. 1995 (Tom95)	6166.44	8717.82
Perrin 86 (Per86)	4435.69	
North et al. 1994 (North94)	6717.69	

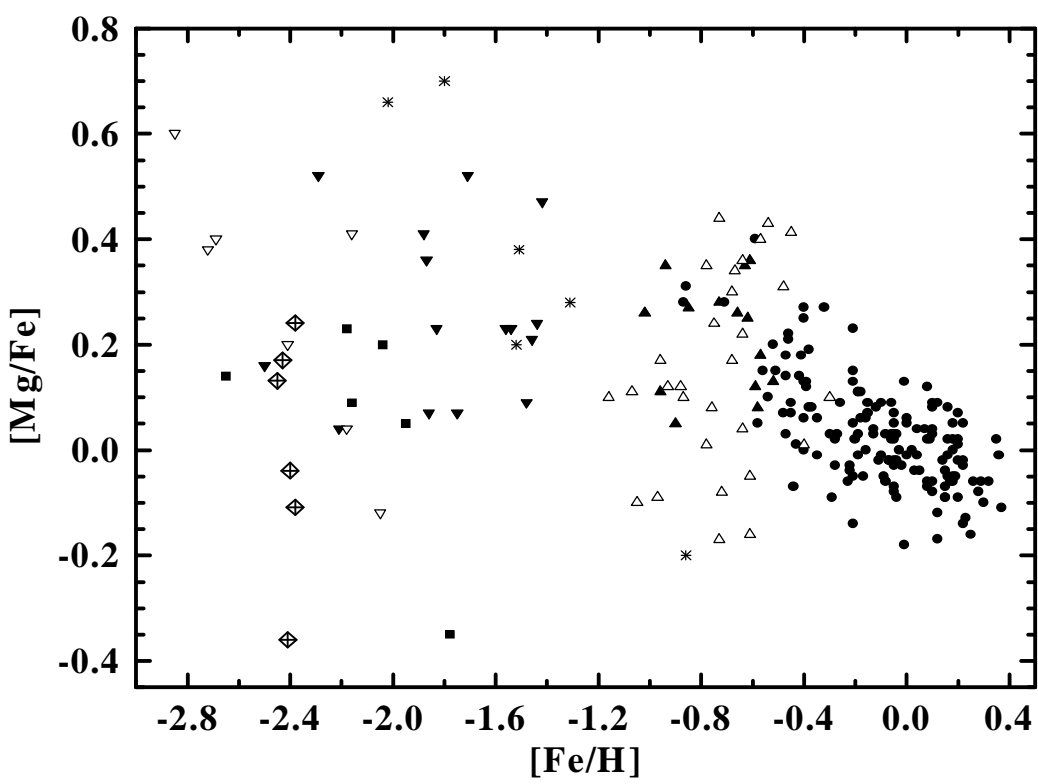
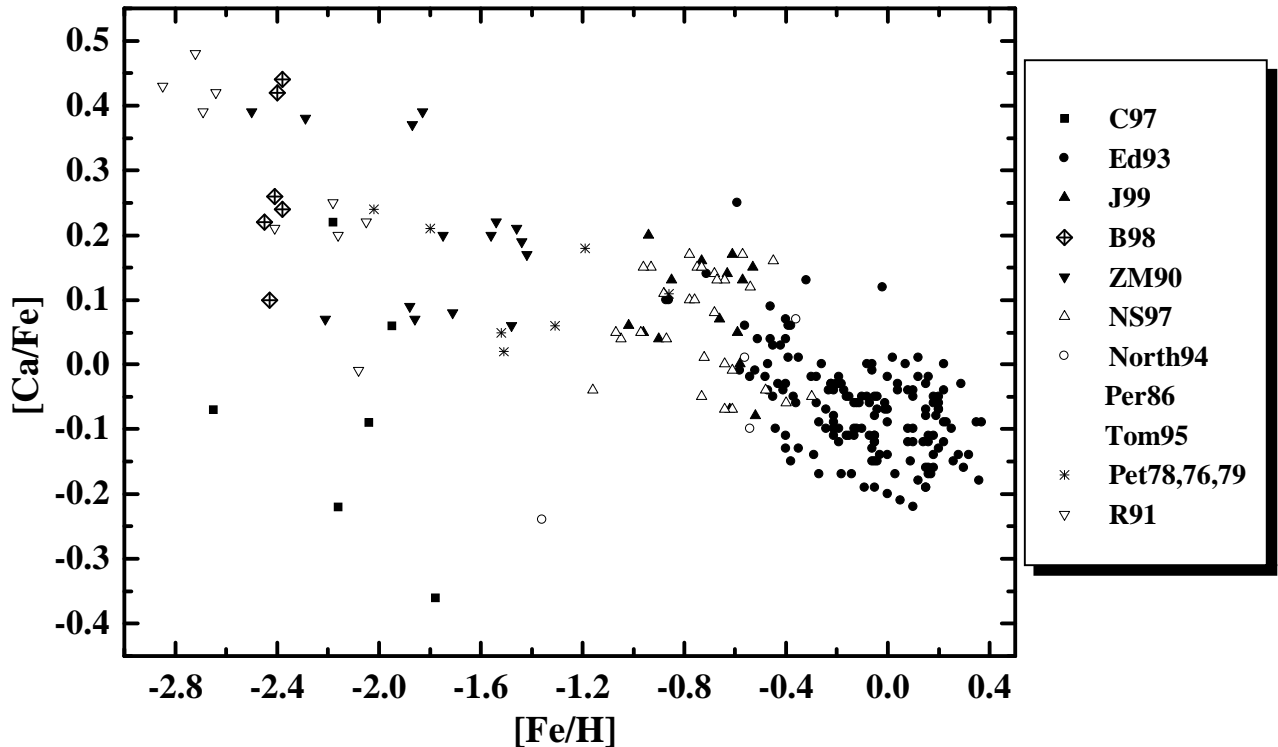


FIGURE 3

TABLE 3
NON-LTE ABUNDANCES FOR 252 STARS

Star	[Fe/H] _(NETL)	[Ca/H] _(NETL)	[Mg/H] _(NETL)	EW reference
BD+80 245	-1.78	-2.14	-2.13	C97
BD+20 3603	-2.04	-2.13	-1.84	C97
G125-64	-2.16	-2.38	-2.07	C97
G182-31	-2.18	-1.96	-1.95	C97
G90-3	-1.95	-1.89	-1.90	C97
G190-15	-2.65	-2.72	-2.51	C97
HD 400	-0.15	-0.26	-0.06	Ed93
HD 739	-0.02	0.1	-0.05	Ed93
HD 2454	-0.21	-0.32	-0.16	Ed93
HD 2615	-0.45	-0.42	-0.36	Ed93
HD 3158	0.08	0.04	0.02	Ed93
HD 3268	-0.13	-0.19	-0.09	Ed93
HD 4307	-0.17	-0.21	-0.22	Ed93
HD 5015	0.10	0.06	0.14	Ed93
HD 6434	-0.38	-0.32	-0.19	Ed93
HD 6920	-0.05	-0.17	-0.02	Ed93
HD 7439	-0.19	-0.29	-0.08	Ed93
HD 7476	-0.09	-0.28	-0.14	Ed93
HD 7570	0.18	0.12	0.13	Ed93
HD 9562	0.2	0.13	0.27	Ed93
HD 9826	0.08	-0.02	0.20	Ed93
HD 10307	0.08	-0.02	0.10	Ed93
HD 12042	-0.22	-0.25	-0.26	Ed93
HD 13555	-0.19	-0.21	-0.08	Ed93
HD 14214	0.15	0.07	—	Ed93
HD 15335	-0.08	-0.13	-0.14	Ed93
HD 15798	-0.10	-0.15	-0.11	Ed93
HD 16673	0.10	0.05	0.19	Ed93
HD 16895	0.08	-0.04	0.01	Ed93
HD 17548	-0.43	-0.46	-0.42	Ed93
HD 19994	0.18	0.13	0.18	Ed93
HD 20807	-0.05	-0.16	-0.08	Ed93
HD 22001	-0.01	-0.08	-0.19	Ed93
HD 22484	0.00	-0.07	-0.01	Ed93
HD 23754	0.16	0.04	0.11	Ed93
HD 25621	0.16	0.00	0.15	Ed93
HD 26491	-0.08	-0.08	-0.05	Ed93
HD 29645	0.16	-0.01	—	Ed93
HD 30562	0.22	0.22	0.27	Ed93
HD 30649	-0.40	-0.36	-0.13	Ed93
HD 30743	-0.21	-0.31	0.02	Ed93
HD 33256	-0.14	-0.31	—	Ed93
HD 33608	0.37	0.28	0.26	Ed93
HD 34411	0.09	-0.06	0.11	Ed93
HD 35296	0.10	8.88	0.18	Ed93
HD 38393	0.00	-0.02	0.06	Ed93
HD 41330	-0.07	-0.18	-0.09	Ed93
HD 43042	0.12	-0.06	-0.05	Ed93

TABLE 3—*Continued*

Star	[Fe/H] _(NETL)	[Ca/H] _(NETL)	[Mg/H] _(NETL)	EW reference
HD 43318	-0.03	-0.17	-0.03	Ed93
HD 43947	-0.19	-0.22	-0.16	Ed93
HD 45701	0.20	0.13	0.11	Ed93
HD 48938	-0.26	-0.26	-0.17	Ed93
HD 49933	-0.27	-0.36	—	Ed93
HD 50223	-0.04	-0.09	-0.13	Ed93
HD 51530	-0.38	-0.53	-0.30	Ed93
HD 55575	-0.21	-0.25	-0.08	Ed93
HD 58551	-0.40	-0.43	-0.27	Ed93
HD 60532	-0.07	-0.13	-0.09	Ed93
HD 61421	0.05	-0.16	0.01	Ed93
HD 67228	0.14	0.02	0.12	Ed93
HD 68284	-0.41	-0.45	-0.23	Ed93
HD 68456	-0.15	-0.20	-0.08	Ed93
HD 69611	-0.40	-0.33	-0.15	Ed93
HD 69897	-0.12	-0.22	—	Ed93
HD 70110	0.12	0.1	0.00	Ed93
HD 74011	-0.46	-0.37	-0.25	Ed93
HD 76151	0.10	-0.12	0.04	Ed93
HD 79028	0.00	-0.20	0.05	Ed93
HD 82328	-0.05	-0.10	-0.13	Ed93
HD 84737	0.15	0.08	0.11	Ed93
HD 86728	0.20	0.15	0.21	Ed93
HD 87141	0.15	-0.04	0.06	Ed93
HD 88737	0.26	0.11	0.20	Ed93
HD 88986	0.04	0.01	0.08	Ed93
HD 89125	-0.24	-0.34	—	Ed93
HD 89707	-0.28	-0.34	-0.26	Ed93
HD 89744	0.28	0.14	0.20	Ed93
HD 91752	-0.13	-0.23	—	Ed93
HD 91889	-0.11	-0.17	-0.13	Ed93
HD 95128	0.04	0.00	0.03	Ed93
HD 95241	-0.16	-0.21	-0.16	Ed93
HD 98553	-0.28	-0.30	-0.31	Ed93
HD 98991	0.00	-0.14	—	Ed93
HD 99747	-0.36	-0.42	—	Ed93
HD 102574	0.22	0.13	0.19	Ed93
HD 102634	0.30	0.14	0.20	Ed93
HD 102870	0.22	0.10	0.08	Ed93
HD 106516	-0.52	-0.53	-0.32	Ed93
HD 107113	-0.35	-0.48	-0.36	Ed93
HD 107213	0.36	0.18	0.35	Ed93
HD 108309	0.15	0.12	0.08	Ed93
HD 108954	0.00	-0.09	—	Ed93
HD 109358	-0.05	-0.20	-0.12	Ed93
HD 110897	-0.37	-0.42	-0.29	Ed93
HD 112164	0.32	0.18	0.26	Ed93
HD 114642	-0.05	-0.24	-0.07	Ed93

TABLE 3—*Continued*

Star	[Fe/H] _(NETL)	[Ca/H] _(NETL)	[Mg/H] _(NETL)	EW reference
HD 114710	0.15	-0.04	0.06	Ed93
HD 114762	-0.56	-0.50	-0.41	Ed93
HD 114837	-0.18	-0.21	-0.07	Ed93
HD 115383	0.12	0.13	0.21	Ed93
HD 115617	0.02	0.03	0.02	Ed93
HD 121370	0.35	0.26	0.37	Ed93
HD 124570	0.17	0.00	0.11	Ed93
HD 124850	-0.05	-0.16	0.02	Ed93
HD 125184	0.23	0.14	0.10	Ed93
HD 127334	0.16	0.14	0.18	Ed93
HD 128167	-0.29	-0.43	-0.38	Ed93
HD 128620	0.20	0.14	0.22	Ed93
HD 130551	-0.48	-0.50	-0.41	Ed93
HD 131117	0.22	0.18	0.20	Ed93
HD 134169	-0.71	-0.57	-0.43	Ed93
HD 136064	0.10	-0.02	0.02	Ed93
HD 136351	0.10	0.00	0.13	Ed93
HD 137052	-0.05	-0.17	0.00	Ed93
HD 141004	-0.01	-0.07	0.12	Ed93
HD 142373	-0.27	-0.44	-0.24	Ed93
HD 142860	-0.06	-0.21	-0.04	Ed93
HD 143761	-0.12	-0.18	-0.04	Ed93
HD 144172	-0.35	-0.34	-0.29	Ed93
HD 144585	0.29	0.26	0.23	Ed93
HD 148211	-0.47	8.88	-0.29	Ed93
HD 148816	-0.51	-0.47	-0.36	Ed93
HD 150177	-0.40	-0.51	-0.40	Ed93
HD 150453	-0.23	-0.27	-0.29	Ed93
HD 151769	0.15	-0.01	—	Ed93
HD 153597	-0.04	-0.19	-0.06	Ed93
HD 155358	-0.47	-0.47	-0.33	Ed93
HD 156098	0.19	0.11	0.14	Ed93
HD 157089	-0.39	-0.33	-0.26	Ed93
HD 157214	-0.32	-0.19	-0.05	Ed93
HD 159307	-0.54	-0.56	-0.44	Ed93
HD 159332	-0.06	-0.19	-0.03	Ed93
HD 160032	-0.16	-0.27	-0.10	Ed93
HD 160933	-0.20	-0.23	-0.18	Ed93
HD 162396	-0.24	-0.31	—	Ed93
HD 163989	-0.05	-0.13	-0.03	Ed93
HD 165908	-0.40	-0.53	-0.34	Ed93
HD 168151	-0.19	-0.31	-0.20	Ed93
HD 169830	0.20	0.07	0.18	Ed93
HD 173667	-0.06	-0.06	—	Ed93
HD 174912	-0.42	-0.39	-0.28	Ed93
HD 175317	0.25	0.15	0.09	Ed93
HD 177565	0.07	0.07	0.11	Ed93
HD 181096	-0.13	-0.24	-0.10	Ed93

TABLE 3—*Continued*

Star	[Fe/H] _(NETL)	[Ca/H] _(NETL)	[Mg/H] _(NETL)	EW reference
HD 184499	-0.59	-0.34	-0.19	Ed93
HD 187013	-0.06	-0.07	0.03	Ed93
HD 187691	0.18	0.07	0.12	Ed93
HD 193307	-0.22	-0.25	-0.25	Ed93
HD 196378	-0.30	-0.32	-0.27	Ed93
HD 198084	0.18	0.02	0.20	Ed93
HD 199289	-0.86	-0.76	-0.55	Ed93
HD 199623	-0.21	-0.31	-0.35	Ed93
HD 200790	0.03	-0.14	-0.01	Ed93
HD 201099	-0.39	-0.38	-0.27	Ed93
HD 201891	-0.87	-0.77	-0.59	Ed93
HD 205294	-0.21	-0.30	-0.26	Ed93
HD 207978	-0.45	-0.50	-0.38	Ed93
HD 208906	-0.58	-0.59	-0.53	Ed93
HD 210752	-0.47	-0.51	-0.44	Ed93
HD 210855	0.18	0.04	0.23	Ed93
HD 215257	-0.44	-0.54	-0.51	Ed93
HD 215648	-0.21	-0.29	-0.06	Ed93
HD 216385	-0.18	-0.35	-0.12	Ed93
HD 217014	0.16	0.05	0.24	Ed93
HD 218470	-0.04	-0.11	-0.01	Ed93
HD 218504	-0.46	-0.42	-0.24	Ed93
HD 222368	-0.10	-0.20	-0.01	Ed93
HD 59984	-0.62	-0.69	-0.37	J99
HD 61902	-0.59	-0.54	-0.47	J99
HD 63077	-0.66	-0.59	-0.40	J99
HD 63598	-0.73	-0.57	-0.45	J99
HD 78747	-0.61	-0.44	-0.25	J99
HD 79601	-0.53	-0.38	—	J99
HD 97320	-1.02	-0.96	-0.76	J99
HD 111971	-0.58	-0.58	-0.50	J99
HD 126793	-0.63	-0.49	-0.28	J99
HD 152924	-0.57	-0.44	-0.39	J99
HD 189558	-0.94	-0.74	-0.59	J99
HD 193901	-0.90	-0.86	-0.85	J99
HD 194598	-0.96	-0.91	-0.85	J99
HD 196892	-0.85	-0.72	-0.58	J99
HD 203608	-0.52	-0.60	-0.39	J99
M92-18	-2.45	-2.23	-2.46	B98
M92-21	-2.38	-2.14	-2.57	B98
M92-34	-2.43	-2.33	-2.33	B98
M92-46	-2.41	-2.15	-2.84	B98
M92-60	-2.40	-1.98	-2.53	B98
M92-350	-2.38	-1.94	-2.24	B98
BD+2 3375	-2.29	-1.91	-1.77	ZM90
BD+3 740	-2.50	-2.11	-2.34	ZM90
BD+17 4708	-1.54	-1.32	-1.31	ZM90
HD 16031	-1.56	-1.36	-1.33	ZM90

TABLE 3—*Continued*

Star	[Fe/H] _(NETL)	[Ca/H] _(NETL)	[Mg/H] _(NETL)	EW reference
HD 19445	-1.88	-1.79	-1.47	ZM90
HD 34328	-1.42	-1.25	-0.95	ZM90
HD 59392	-1.44	-1.25	-1.20	ZM90
HD 74000	-1.83	-1.44	-1.60	ZM90
HD 84937	-1.86	-1.79	-1.79	ZM90
HD 116064	-1.87	-1.50	-1.51	ZM90
HD 140283	-2.21	-2.14	-2.17	ZM90
HD 160617	-1.48	-1.42	-1.39	ZM90
HD 166913	-1.46	-1.25	-1.25	ZM90
HD 181743	-1.71	-1.63	-1.19	ZM90
HD 213657	-1.75	-1.55	-1.68	ZM90
BD-21 3420	-0.88	-0.77	-0.76	NS97
CD-33 3337	-1.16	-1.2	-1.06	NS97
CD-45 3283	-0.72	-0.71	-0.80	NS97
CD-47 1087	-0.64	-0.51	-0.28	NS97
CD-57 1633	-0.73	-0.78	-0.90	NS97
CD-61 0282	-0.97	-0.92	-1.06	NS97
G005-040	-0.68	-0.54	-0.38	NS97
G046-031	-0.61	-0.68	-0.66	NS97
G088-040	-0.64	-0.64	-0.42	NS97
G102-020	-0.93	-0.78	-0.81	NS97
HD 3567	-1.05	-1.01	-1.15	NS97
HD 17288	-0.75	-0.6	-0.51	NS97
HD 17820	-0.54	-0.42	-0.11	NS97
HD 22879	-0.67	-0.54	-0.33	NS97
HD 24339	-0.48	-0.52	-0.17	NS97
HD 25704	-0.68	-0.60	-0.51	NS97
HD 76932	-0.73	-0.58	-0.29	NS97
HD 83220	-0.40	-0.46	-0.39	NS97
HD 103723	-0.61	-0.62	-0.77	NS97
HD 105004	-0.64	-0.71	-0.60	NS97
HD 106038	-1.07	-1.02	-0.96	NS97
HD 113083a	-0.78	-0.68	-0.77	NS97
HD 113083b	-0.76	-0.66	-0.68	NS97
HD 113679	-0.45	-0.29	-0.037	NS97
HD 120559	-0.78	-0.61	-0.43	NS97
HD 121004	-0.57	-0.40	-0.17	NS97
HD 126681	-0.96	-0.81	-0.79	NS97
HD 241253	-0.87	-0.83	-0.77	NS97
W7547	-0.30	-0.35	-0.20	NS97
HD 48565	-0.54	-0.64	—	North
HD 147609	-0.36	-0.29	—	North
HD 99383	-1.36	-1.60	—	Per86
BD+26 3578	-2.02	-1.78	-1.36	Pet76
BD+34 2476	-1.80	-1.59	-1.10	Pet78
HD 64090	-1.52	-1.47	-1.32	Pet78
HD 94028	-1.31	-1.25	-1.03	Pet78
HD 97916	-0.86	-0.75	-1.06	Pet78

TABLE 3—*Continued*

Star	[Fe/H] _(NETL)	[Ca/H] _(NETL)	[Mg/H] _(NETL)	EW reference
HD 108177	-1.51	-1.49	-1.13	Pet78
HD 103095	-1.19	-1.01	—	Pet79
BD-33 1173	-2.69	-2.3	-2.29	R91
BD-13 3442	-2.72	-2.24	-2.34	R91
CD-71 1234	-2.05	-1.83	-2.17	R91
NLTT56-75	-2.41	-2.20	-2.21	R91
NLTT635-14	-2.18	-1.93	-2.14	R91
NLTT732-48	-2.08	-2.09	—	R91
NLTT815-43	-2.64	-2.22	—	R91
NLTT831-70	-2.85	-2.42	-2.25	R91
NLTT R740	-2.16	-1.96	-1.75	R91
HD 6582	-0.56	-0.55	-0.52	Tom95
Sun	0	0	0	

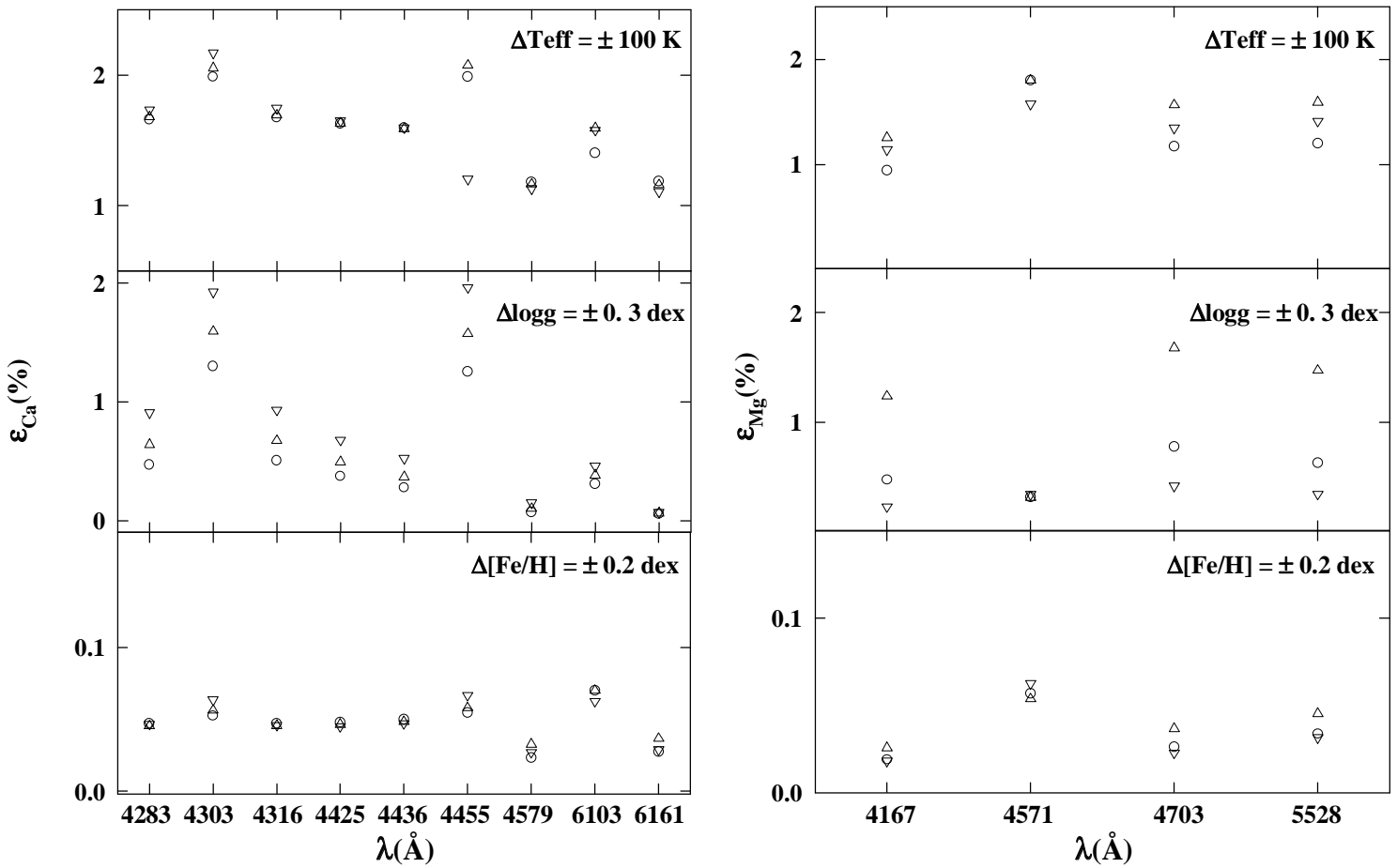


FIGURE 4

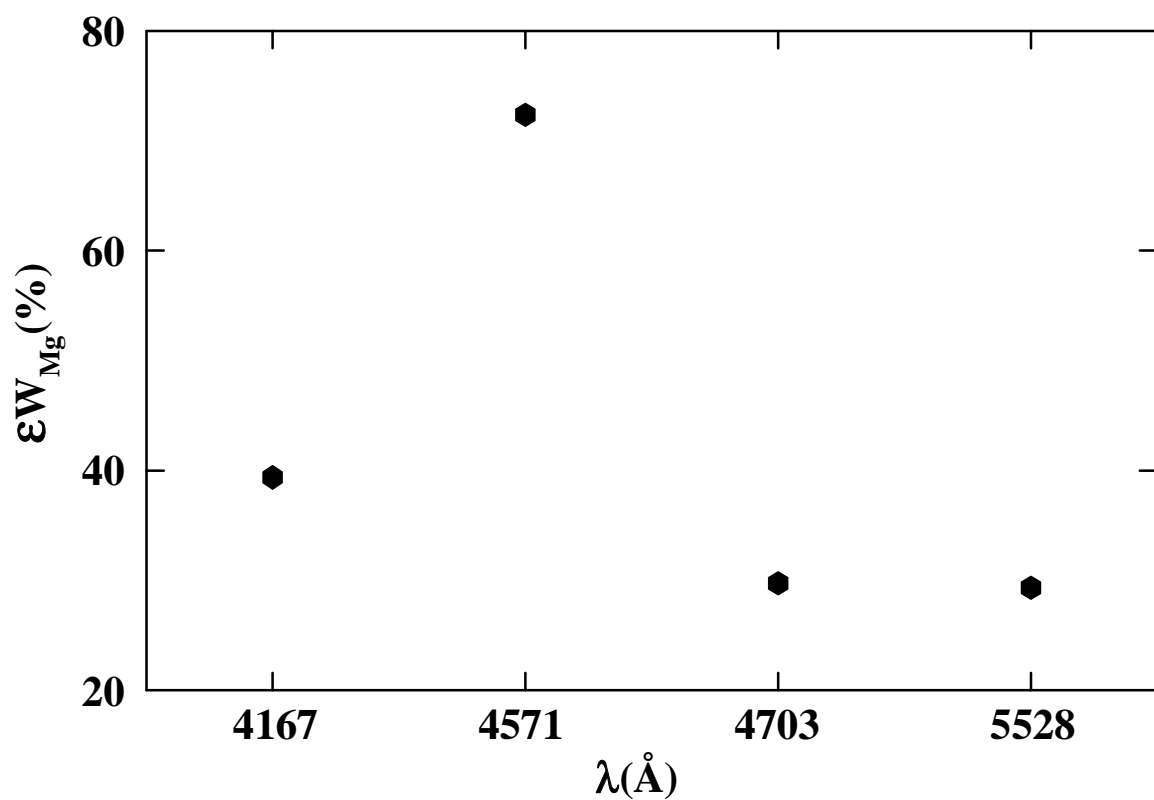
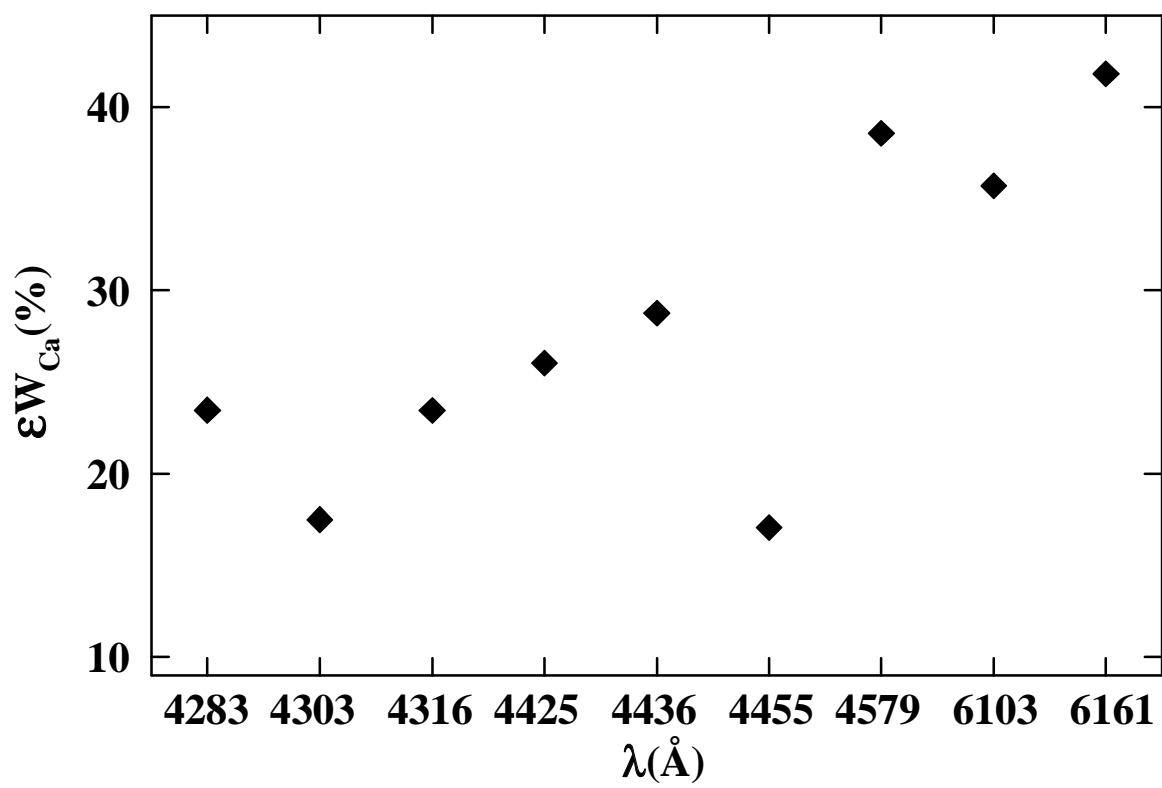


FIGURE 5

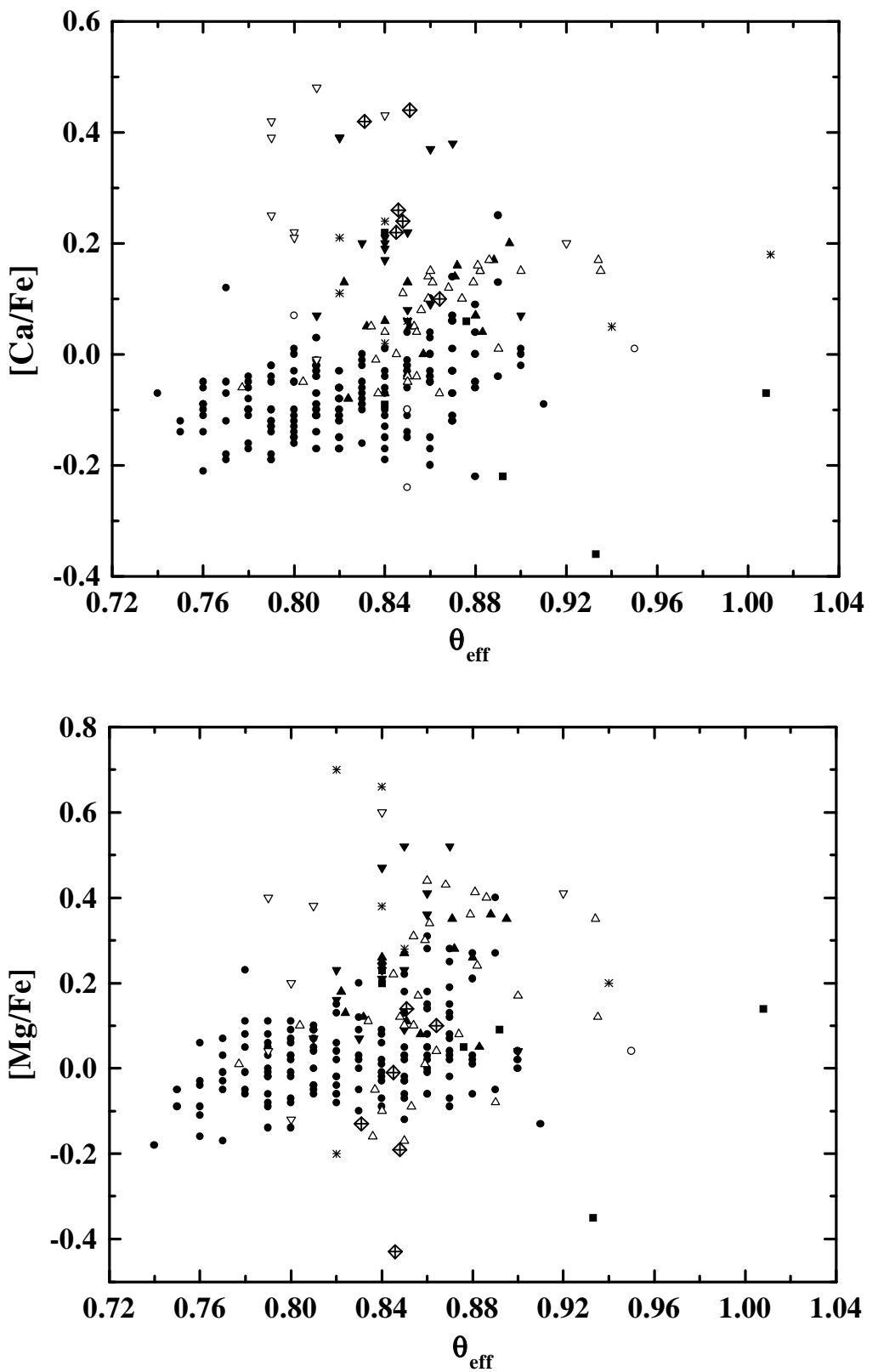


FIGURE 6

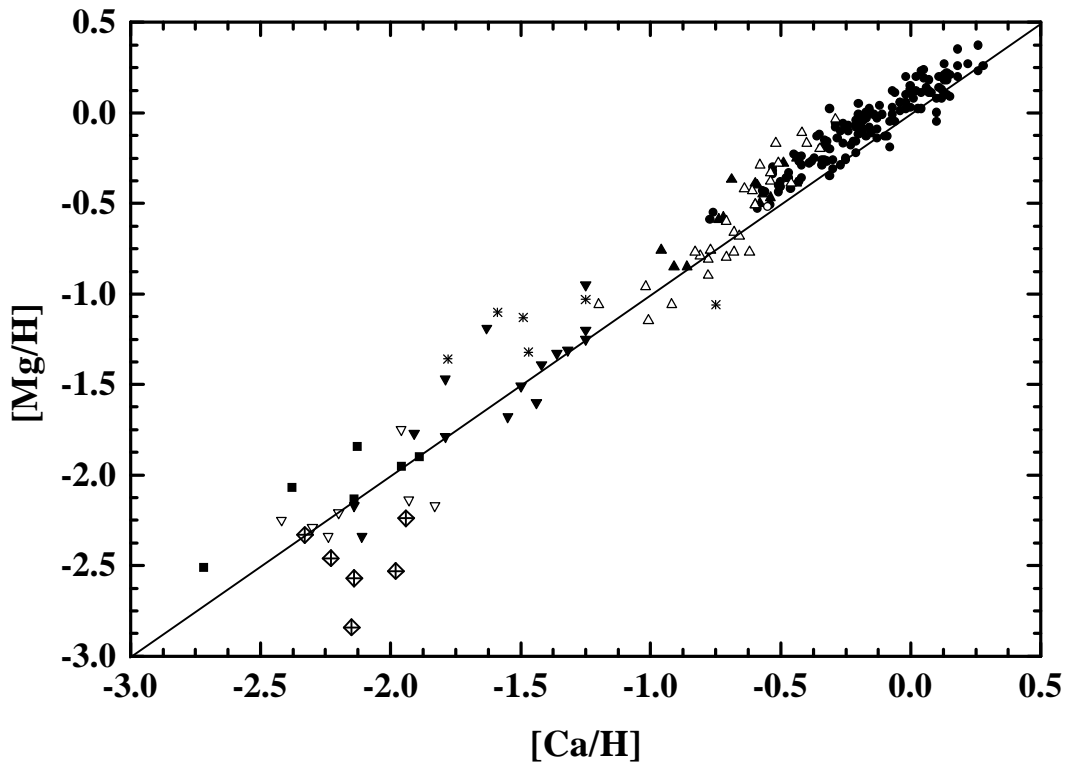


FIGURE 7